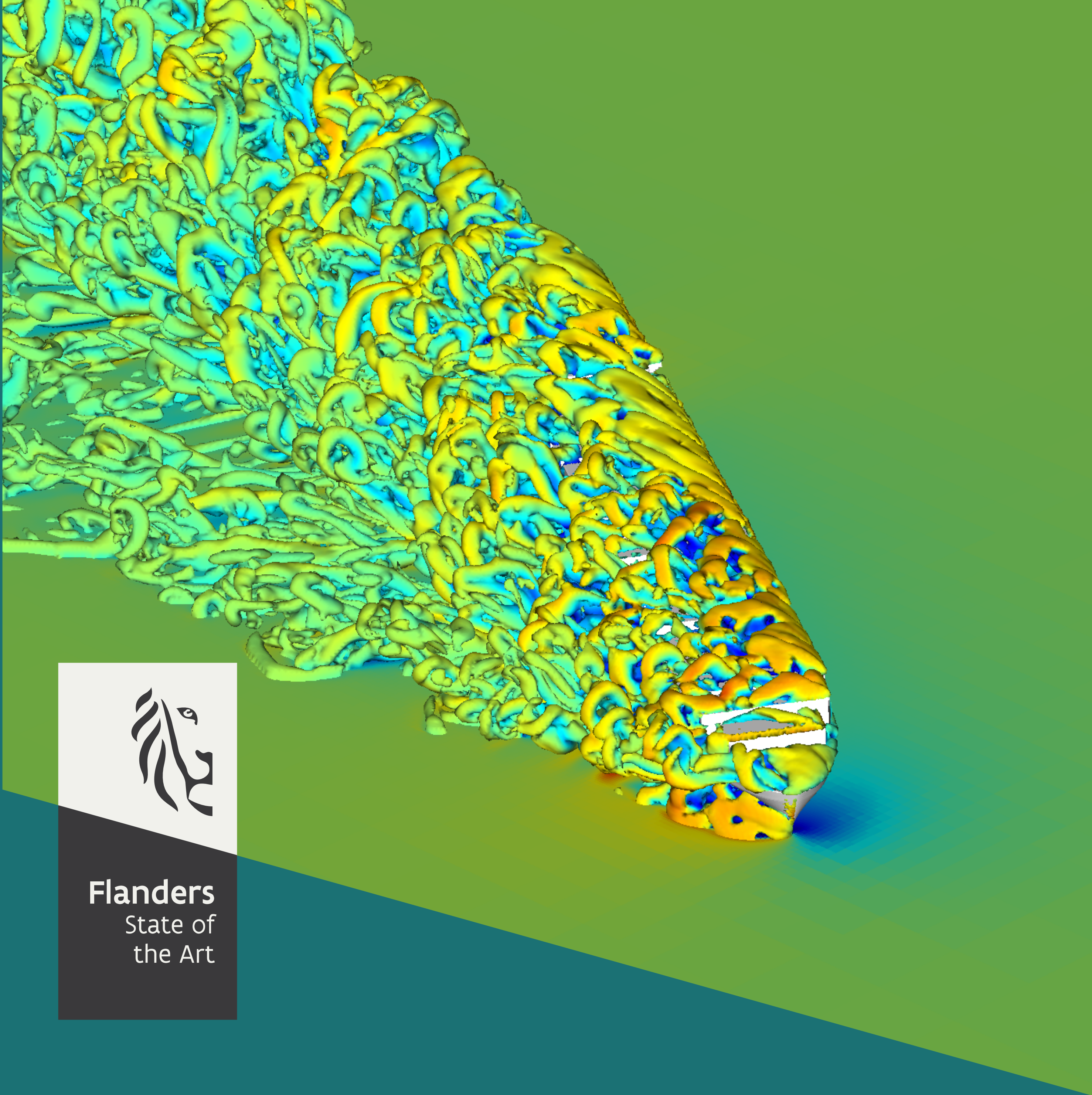

Flanders
State of
the Art

17_025_1
FH Reports

Computation of Rudder Open Water Characteristics

Charles Darwin (H40)

DEPARTMENT
MOBILITY &
PUBLIC
WORKS

www.flandershydraulics.be

Computation of Rudder Open Water Characteristics

Charles Darwin (H40)

Van Hoydonck, W.; Panahi, S.; López Castaño, S.; Eloot, K.

Flanders Hydraulics
Flanders
State of the Art

Cover figure © The Government of Flanders, Department of Mobility and Public Works, Flanders Hydraulics

Legal notice

Copyright and citation

D/2024/3241/100

This publication should be cited as follows:

Van Hoydonck, W.; Panahi, S.; López Castaño, S.; Eloot, K. (2024). Computation of Rudder Open Water Characteristics: Charles Darwin (H40). Version 3.0. FH Reports, 17_025_1. Flanders Hydraulics: Antwerp

Document identification

Customer:	Flanders Hydraulics	Ref.:	WL2024R17_025_1
Keywords (3-5):	Open water rudder characteristics, CFD, Charles Darwin		
Knowledge domains:	Harbours and waterways > Manoeuvring Behaviour > Open water > Numerical calculations		
Text (p.):	13	Appendices (p.):	2
Confidential:	No	☒ Available online	

Author(s):	Van Hoydonck, W.

Control

	Name	Signature
Revisor(s):	Panahi, S.; López Castaño, S.; Eloot, K.	Getekend door:Katrien Eloot (Signature) Getekend op:2024-09-05 16:05:16 +02:00 Reden:Ik keur dit document goed Eloot Katrien Vlaamse overheid Getekend door:Santiago LOPEZ CASTAÑ Getekend op:2024-09-06 16:00:10 +02:00 Reden:Ik keur dit document goed Lopez Castano Santiago Vlaamse overheid Getekend door:Saeid PANAHI (Signature) Getekend op:2024-09-10 17:22:19 +02:00 Reden:Ik keur dit document goed Panahi Saeid Vlaamse overheid
Project leader:	Van Hoydonck, W.	Getekend door:Wim Van Hoydonck (Sign Getekend op:2024-09-06 10:50:46 +02:0 Reden:Ik keur dit document goed Van Hoydonck Wim Vlaamse overheid

Approval

Head of division:	Bellafkih, A.	Getekend door:Abdelkarim Bellafkih (Sign Getekend op:2024-09-05 16:13:33 +02:0 Reden:Ik keur dit document goed Bellafkih Abdelkarim Vlaamse overheid

Abstract

The objective of this report is to document the procedure to determine open-water rudder characteristics using the Computational Fluid Dynamics (CFD) software package FINE/Marine. In the current report, open-water rudder characteristics for the vessel *Charles Darwin* are determined. The approach that is used here follows a setup that is similar to what was reported in the past (Van Hoydonck *et al.*, 2018), although now with some simplifications: for the current setup, the domain consists of a single cylinder. A far field velocity boundary condition is defined at the domain boundaries and the rudder rotation is imposed by rotating the complete domain together with the rudder. In Van Hoydonck *et al.* (2018), a sliding grid approach was used with an inner and outer domain to accomplish this.

The results show correct qualitative behaviour for the lift and drag force of the rudder both in normal flow conditions as well as in reverse flow conditions. The numerically estimated lift curve slope in normal flow conditions is shown to agree very well with a theoretical estimate of the slope. The coefficient values are interpolated to one and five degree increments with very little difference between the interpolations.

Contents

List of Figures

List of Tables

Nomenclature

Abbreviations

CAD	Computer Aided Design
CFD	Computational Fluid Dynamics
DES	Detached Eddy Simulation
FH	Flanders Hydraulics
LES	Large Eddy Simulation

Latin symbols

$\mathcal{R}$	Aspect ratio, $\frac{b^2}{S}$	—
b	Rudder height	m
c	Rudder chord length	m
C_L	Lift coefficient	—
C_{L_α}	Wing lift curve slope	1/rad
C_{l_α}	Airfoil lift curve slope	1/rad
L_{ref}	Reference length	m
N	Yawing moment coefficient	—
Re	Reynolds number	—
S	Rudder surface area	m^2
t/c	Thickness	%
V_{ref}	Reference velocity	m/s
X	longitudinal force coefficient	—
Y	lateral force coefficient	—

Greek symbols

α	Angle of attack	rad
δ	Wing planform efficiency	—
μ	Dynamic viscosity	Pas
ρ	Fluid density	kg/m^3
ω	Angular velocity	rad/s

1 Introduction

For the derivation of mathematical models of vessels for use in the ship simulators at Flanders Hydraulics (FH), towing tank tests are executed to determine the behaviour of a vessel for a range of parameters such as under keel clearance, velocity, drift angle, proximity to walls, propeller rate and rudder deflection (Van Kerkhove *et al.*, 2009). As part of this program, tests are executed to determine the forces and moments acting on the rudder in open water conditions, where the influence of the ship hull is non-existing and the effects of the proximity of the water surface, tank walls and bottom are minimal (Vantorre, 2001). Together with the open water characteristics of the propeller, this data is used to derive mathematical manoeuvring models for use in the simulators at FH. For symmetrical rudders, the rudder forces are determined by rotating the rudder with respect to the oncoming flow from 0 to 180 degrees. The rudder is rotated in the opposite direction as well (from 180 to 0 degrees) and the rudder longitudinal force, lateral force and yawing moment are determined by averaging of both results.

1.1 Ship and rudder geometry

In project 23_074 (Onderzoek voor toegankelijkheid supply schepen tot haven van Oostende), a manoeuvring model will be developed for the hopper dredger *Charles Darwin* (see Fig. 1) based on towing tank tests. For the derivation of the mathematical model, the rudder open water characteristics are required. The ship is equipped with two ducted propellers and two symmetrical rudders with a flap that both have a toe-out of five degrees. For the scale model research, the rudder geometry is simplified to a single solid surface as shown in Fig. 2a. For the determination of open-water characteristics, a mirror plane is assumed at the rudder top, which means that the geometry for the actuation of the rudder flap above the rudder top surface was removed (see Fig. 2b).

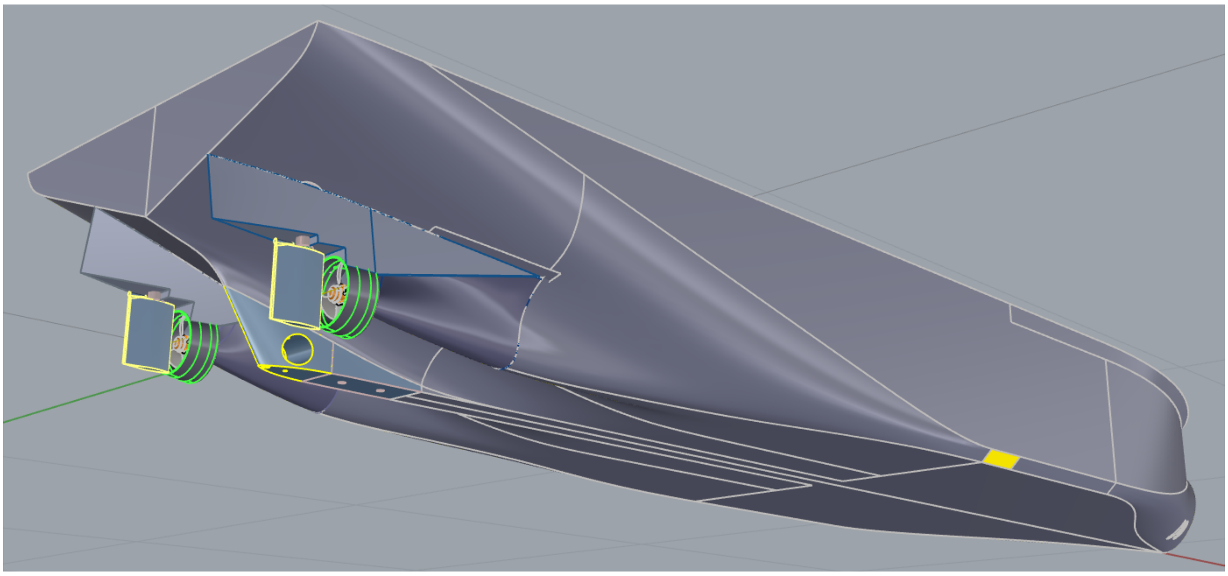

Figure 1 – Perspective view of scale 3D CAD model of Charles Darwin hull.

The rudder characteristics of the simplified geometry are listed in Table 1. The rudder geometry does not contain twist, taper nor sweep. The reference point for the force computation is taken at the centre of the rudder stock, at $x = 0.41$ c.

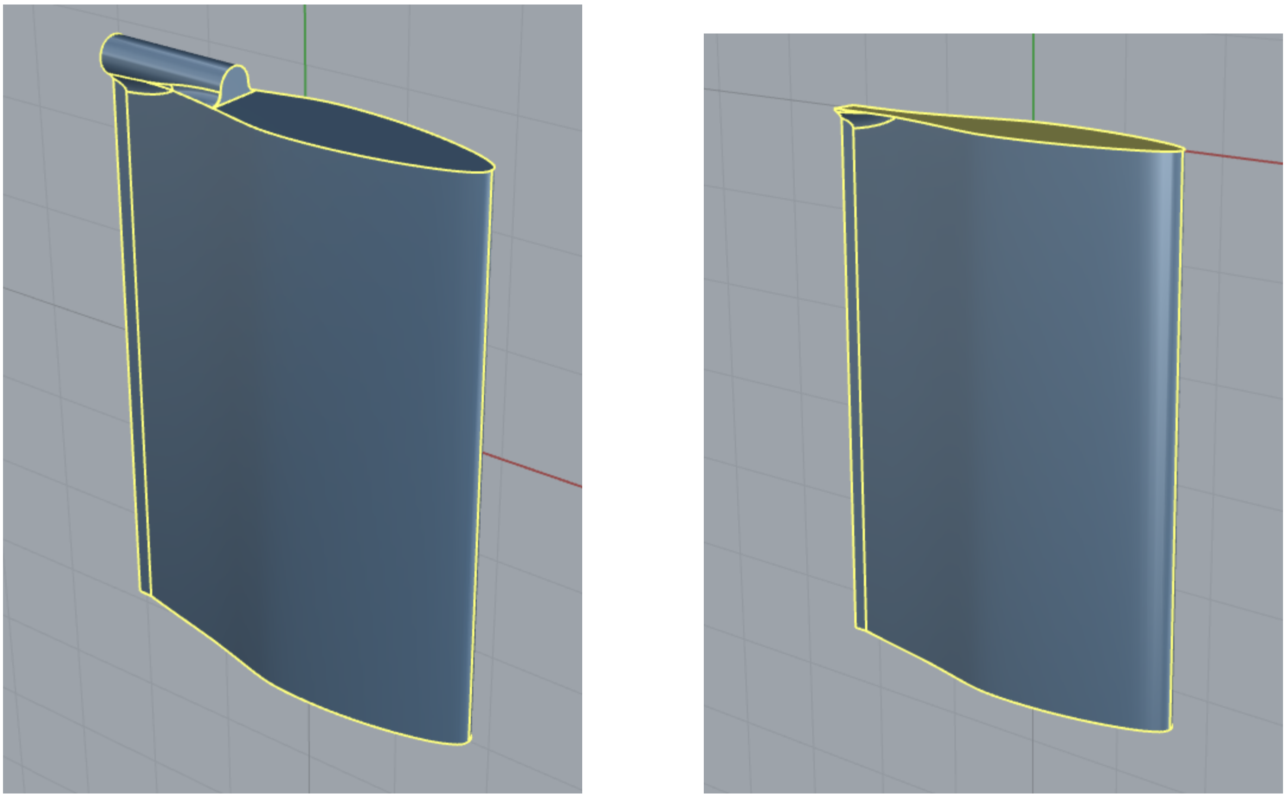

(a) Scale model Computer Aided Design (CAD) geometry. (b) Full scale CAD model for CFD computations.

Figure 2 – Perspective view of Charles Darwin rudder CAD model.

Table 1 – Geometric characteristics of the full scale rudder.

characteristic	symbol	value
chord	c	3.9 m
height	b	5.4 m
thickness	t/c	$22\,\%$
area	S	21.06 m^2
aspect ratio	AR	1.38

1.2 Operating conditions

The flow is assumed to be standard ITTC fresh water with a temperature of 15 °C with density $\rho = 999.1026$ kg/m^3 and dynamic viscosity $\mu = 0.001\,138$ Pas. Computations are executed at full scale in unsteady mode, with reference speed $V_{ref} = 5$ m/s using the chord as reference length $L_{ref} = 3.9$ m, The rudder is rotated in the flow with an angular velocity $\omega = 1$ °/s. The Reynolds number Re based on the rudder chord and reference speed is $Re = \frac{\rho V_{ref} c}{\mu}$ = 17.12×10^6.

The curves of the lift, drag and pitch moment coefficients are generated by averaging the values of two curves obtained with the rudder angle of attack increasing and decreasing. Due to the symmetry of the rudder foil, a single computation with α in the range $0°$ to $360°$ is sufficient to generate the data for both increasing and decreasing angle of attack. This averaging is required because the angular velocity is not low enough to prevent hysteresis. Reducing the angular velocity by an order of magnitude might solve that issue, but that would mean that the simulation times would increase by a factor ten (all else being equal) which is likely too long.

1.3 Estimation of rudder lift curve slope in attached flow conditions

In attached flow conditions, the lift curve slope of a wing C_{L_α} (and hence, the lift coefficient value at a certain angle of attack α) can be determined analytically using the two-dimensional lift curve slope of the foil section C_{l_α} and some geometric parameters of the wing.

In Rhino, a cross section of the airfoil was extracted from the 3D CAD model and modified to give it a sharp trailing edge (see Fig. 3). It's chord length was normalised and the x and y coordinates saved to a text file.

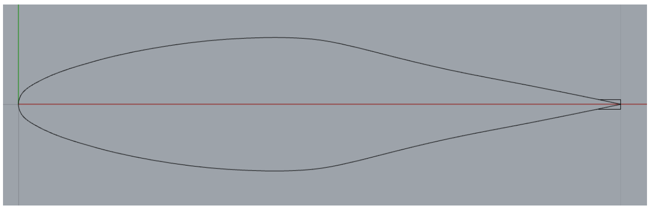

Figure 3 – Original (blunt trailing edge) and modified (sharp trailing edge) rudder profile for computing 2D hydrodynamic characteristics.

1.3.1 XFOIL computations

The airfoil geometry was imported in XFOIL (Fig. 4), and the panel distribution optimized ($N = 160$ panels) in the PPAR menu.

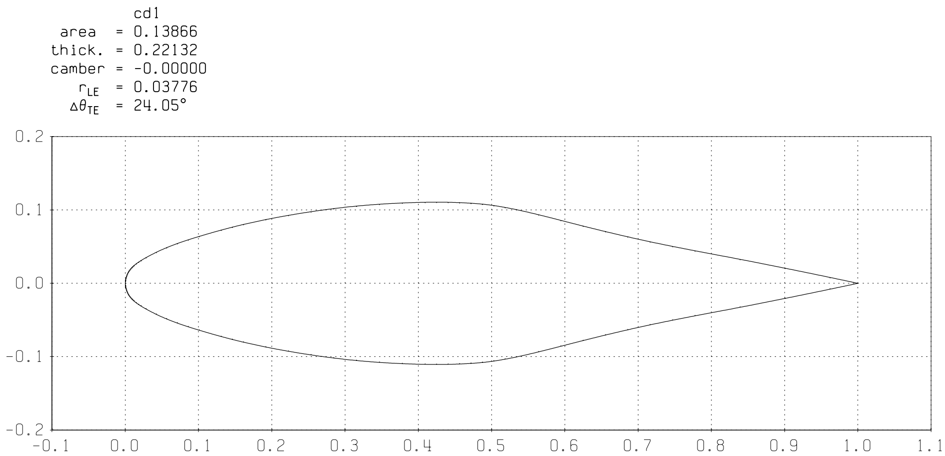

Figure 4 – Rudder imported in XFOIL

In the OPER menu, the viscous option is selected and Re is set to 17.12×10^6. The location on the airfoil upper and lower surfaces where the boundary layer is forced to transition from laminar to turbulent flow is set to $x = 0.1$ (through the VPAR menu). The resulting values at α = $1°$ and $2°$ for the lift, drag and pitching coefficient are shown in Fig. 5.

1.3.2 Estimation of rudder lift curve slope

The airfoil (2D) lift curve slope is computed with a finite difference approximation using the data in Fig. 5:

$$C_{l_\alpha} = \frac{0.2134 - 0.1070}{2 - 1} \frac{180}{\pi} \approx 6.06. \quad (1)$$

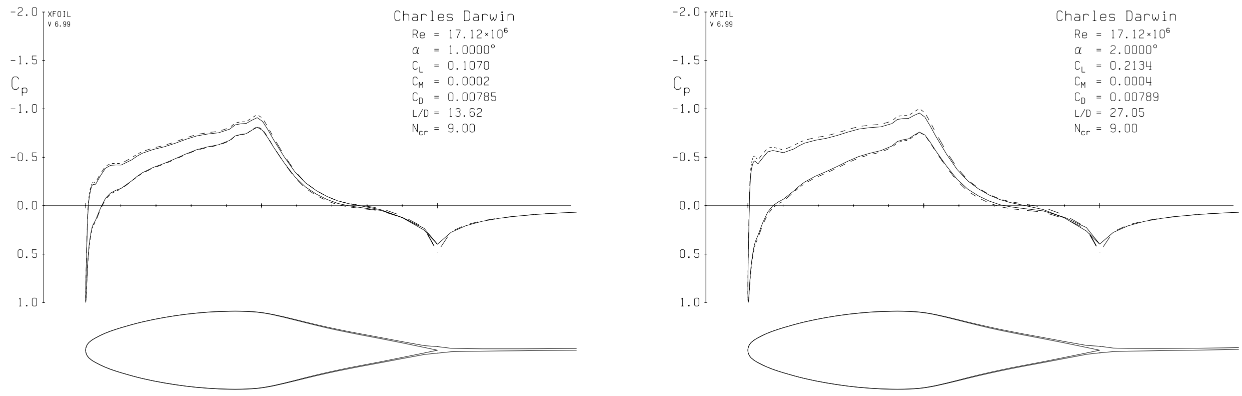

Figure 5 – 2D Viscous solution around the rudder foil at $\alpha = 1°$ (left) and $\alpha = 2°$ (right).

Due to the use of a symmetry condition at the rudder top side, the surface area and aspect ratio must be calculated using $2b$ instead of b. Hence, $Æ = 2.76$ is used for the estimation of the 3D lift curve slope C_{L_α} (Leishman, 2023),

$$C_{L_\alpha} = \frac{C_{l_\alpha}}{1 + \frac{(1+\delta)C_{l_\alpha}}{\pi Æ}}, \tag{2}$$

where δ is the spanwise efficiency factor, which for a rectangular wing, is $\delta \approx 0.1$.

Plugging in all known values, it follows that $C_{L_\alpha} = 3.55$. As a consequence, for $\alpha = 5°$ and $\alpha = 10°$, lift coefficients values are $C_L|_{\alpha=5°} = 0.31$ and $C_L|_{\alpha=10°} = 0.62$, respectively.

The results obtained in this section are used as a means to validate the CFD computations that are documented in the next chapter.

1.4 Postprocessing

The longitudinal force X, the lateral (lift) force Y and yawing moment N (around the Z-axis) are required as non-dimensional coefficients. These are obtained from the output of FINE/Marine as follows:

$$X = \frac{F_x}{\frac{1}{2}\rho V_{ref}^2 L_{ref} b}, \tag{3}$$

$$Y = \frac{F_y}{\frac{1}{2}\rho V_{ref}^2 L_{ref} b}, \tag{4}$$

$$N = \frac{M_z}{\frac{1}{2}\rho V_{ref}^2 L_{ref}^2 b}. \tag{5}$$

For small positive angles of attack, the lift will be positive and the drag force negative. The reference point for the force computation is located significantly aft of the quarter chord point (almost at $0.41c$ – near the point of maximum thickness) from which follows that for small positive angles of attack, the yawing moment will be positive.

2 CFD computations

2.1 Domain and mesh setup

2.1.1 Domain size

The rudder is placed in a cylindrical domain with radius $R = 60$ m and height $h = 48$ m, with the rudder top surface aligned with the upper surface of the cylinder, see Fig. 6. The centre of the rudder stock at the upper side of the rudder coincides with the origin of the global axes system of FINE/Marine. The hydrodynamic forces and moments acting on the rudder are resolved in the global axes system of FINE/Marine (see Fig. 7). This means that the longitudinal force X will be negative, and that $D = -X$. The lateral force (L, lift) is positive to port side. The yawing moment is defined around the Z-axis and is positive when it tends to increase the angle of attack α (itself also defined around the positive Z-axis) of the rudder.

The initial Cartesian mesh has $30 \times 30 \times 12$ cells. It follows that the cells of the initial Cartesian grid have edges that are approximately equal in length to the rudder chord. The cell sizes as function of refinement level are shown in Table 2. The smallest geometric feature of the rudder is the width of the trailing edge, which equals 0.0621 m. As a consequence, the maximum refinement should be eight or higher to capture the trailing edge with at least four cells over the width.

Table 2 – Cell sizes as a function of subdivision level.

refinement level	cell size
0	4.0
1	2.0
2	1.0
3	0.5
4	0.25
5	0.125
6	0.0625
7	0.031 25
8	0.015 625
9	0.007 812 5
10	0.003 906 25

2.1.2 Mesh refinement

The grid is constructed using a combination of surface refinements, edge refinements and volumic refinements. The rudder side surfaces and the bottom surface are refined seven times. The rudder trailing edge and the small surfaces adjacent to the trailing edge surface are refined nine times. The complete edge surrounding the bottom rudder surface is refined eight times. The intersection of the rudder with the domain top surface is refined nine times. From the cylindrical domain surfaces, only the top domain is refined (two refinements), following the recommended practices for computations using a rigid lid approximation for the free surface. A volumic refinement is added to refine the computational grid around the rudder. A refinement sector is added with a height of 6 m and a maximum radius of 4 m. Within this volume, the cells are refined five times.

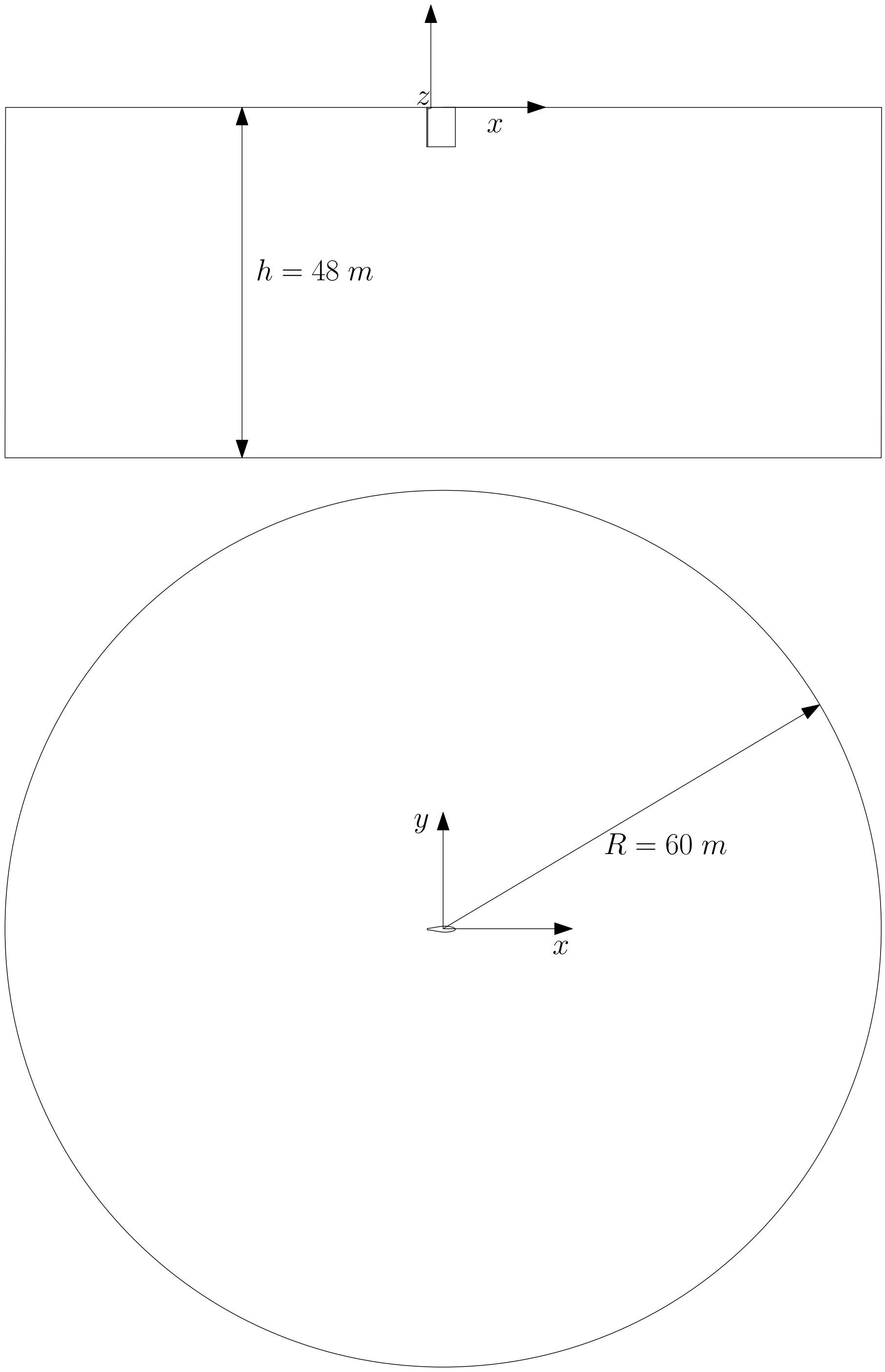

Figure 6 – Side view and top view of the computational domain.

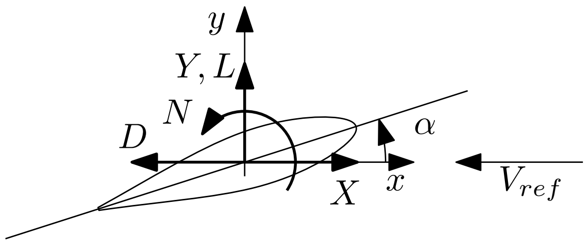

Figure 7 – View of the rudder from above: definition of rudder forces and yawing moment.

2.1.3 Edge snapping and optimization

All edges are captured in the snapping phase of the mesh generation. For buffer insertion, the top and bottom circular edges of the domain have type II while the edges of the rudder itself have type I. In the optimization step, all settings were left at their default values.

2.1.4 Viscous layers

Because forces on the rudder are required for the full range of angles of attack (including conditions with massive flow separation), wall functions are not used. Instead, the viscous layers are resolved ($y+ < 0.8$). Using a reference length of 3.9 m, a reference velocity of 5 m/s and a kinematic viscosity $\nu = 1.1 \times 10^{-6}$ m^2/s, the first layer thickness estimate of HEXPRESS is 7.8×10^{-6} m. For the rudder side surfaces and the bottom surface, 37 layers are required, while the other (smaller) rudder surfaces need 30 layers. For some of the small surfaces, the actual layer count that is inserted is somewhat higher (31 or 32).

After insertion of the viscous layers, the grid consists of $7\,252\,446$ hexagonal cells with a minimum orthogonality of 14.42.

Fig. 8 shows the computational grid on the domain mirror face (top left), a horizontal cut at the vertical centre of the rudder (at $z = -2.7$ m) (top right) and the surface grid on the rudder (bottom).

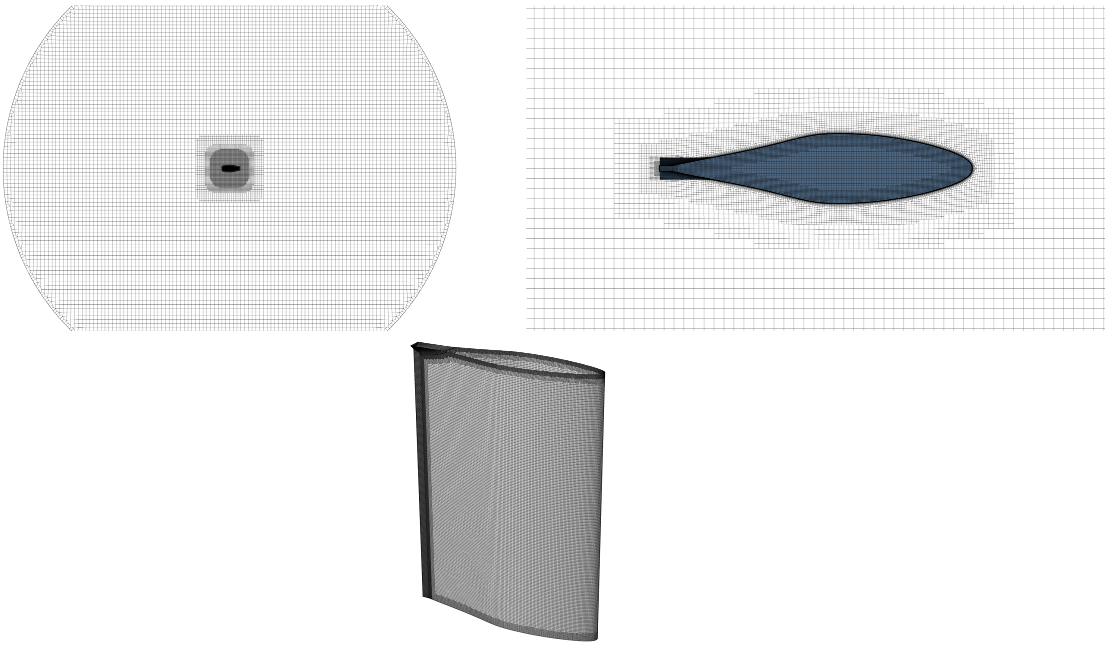

Figure 8 – Visualisations of the computational grid.

2.2 Solver settings

As stated in the previous chapter, due to the symmetry of the rudder, only one computation must be executed to obtain results with both increasing and decreasing angle of attacks. However, due to an unexpected crash in the first computation shortly after the rudder had executed $180°$ out of the total of $360°$, a second computation was configured where the sign of the inflow at the domain boundaries was reversed to run a computation starting from $\alpha = 180°$.

Computations are run in unsteady mode using a single phase. Fully turbulent flow is assumed, using the $k\omega$ SST 2003 turbulence model. The reference length equals the rudder chord, $L_{ref} = 3.9$ m, while the reference speed equals the velocity magnitude of the far field flow, $V_{ref} = 5$ m/s.

The boundary condition on the rudder surface is no-slip to resolve boundary layer flow. *Prescribed pressure - frozen pressure* is used on the domain bottom, while for the cylinder side, a far field velocity condition is used with the x-component equal to $V_x = -5$ m/s. For the second computation, this latter value is negated.

A solid body is defined using the surfaces of the rudder and for this body the rotational degree of freedom around the z-axis is imposed with a *classic ramp*. The settings are such that at $t = 2$ s, the rotation rate is smoothly increased from 0 °/s to 1 °/s at $t = 4$ s.

The flow field in the entire domain is initiated to -5 m/s. Turbulence quantities are left at their default values for the boundary conditions and the initial conditions.

Computations are run in unsteady mode with a time step of $\Delta t = 0.01$ s. The first one was supposed to run $38\,000$ steps, but it crashed during time step $18\,977$. The second computation was configured to run $19\,000$ steps, with the relative linear velocity defined as $V_x = 5$ m/s. During each time step, a maximum of eight non-linear iterations are executed. Dynamic switching between the PCGSTAB_MB and BoomerAMG pressure solvers is activated (by default).

Forces on the rudder geometry are resolved in the global reference frame (not rotating with the rudder) at the centre of the rudder shaft at the rudder top surface (see also Fig. 6).

In addition to the two unsteady computations, some additional steady computations have been executed (at $\alpha = 0°,\ 5°,\ 10°,\ 15°,\ 20°,\ 85°,\ 90°,\ 95°,\ 180°,\ 185°,\ 190°$ and $195°$) to compare with the results of the averaged values of unsteady computations. Note that for angles of attack larger than or equal to $15°$, Xfoil predicts a significant zone of recirculation on the suction side of the airfoil aft of the point of maximum thickness. This means that the assumption of steady flow for these and larger angles of attack may not result in extremely accurate results.

A grid convergence study is not executed for this case as it is similar in setup as the computations reported in Van Hoydonck *et al.* (2018).

2.3 Results

Fig. 9 shows the unsteady results of the first and second computation (subscripts $_{u,1}$ and $_{u,2}$, respectively) as well as the steady results (subscript $_s$). These results show a significant amount of hysteresis near stall (starting at $\alpha = 15°$) due to the large differences in $C_{L,max}$ between increasing and decreasing angle of attack.

These results are further processed to remove overlaps in the angle of attack ranges of both unsteady computations. For each force component, the resulting curves are combined in a single curve that covers the complete range of angles of attack and those series are duplicated and reversed to be able to compute averages. Note that for Y and N, the values of the duplicates are negated. The mean of these two is then computed and those are shown in Fig. 10 as thin black lines. The filled areas show the effect of hysteresis near stall, as well as differences in the longitudinal force coefficient between $30°$ and $90°$ and $95°$ and $170°$. There is also some effect of hysteresis visible in the yawing moment coefficient near stall, but not nearly as significant as for the lateral force. For comparison purposes, the results of the steady computations are shown as dots.

A subset of the complete data ($\alpha = 0°$ to $30°$) is shown in Fig. 11, which shows that the agreement between the steady and averaged unsteady result for the longitudinal force coefficient X is almost perfect until $\alpha = 20°$. The agreement is good for the yawing moment N until $\alpha = 10°$ and deteriorates for larger angles of attack. A similar observation can be made for the lateral (lift) force coefficient (Y).

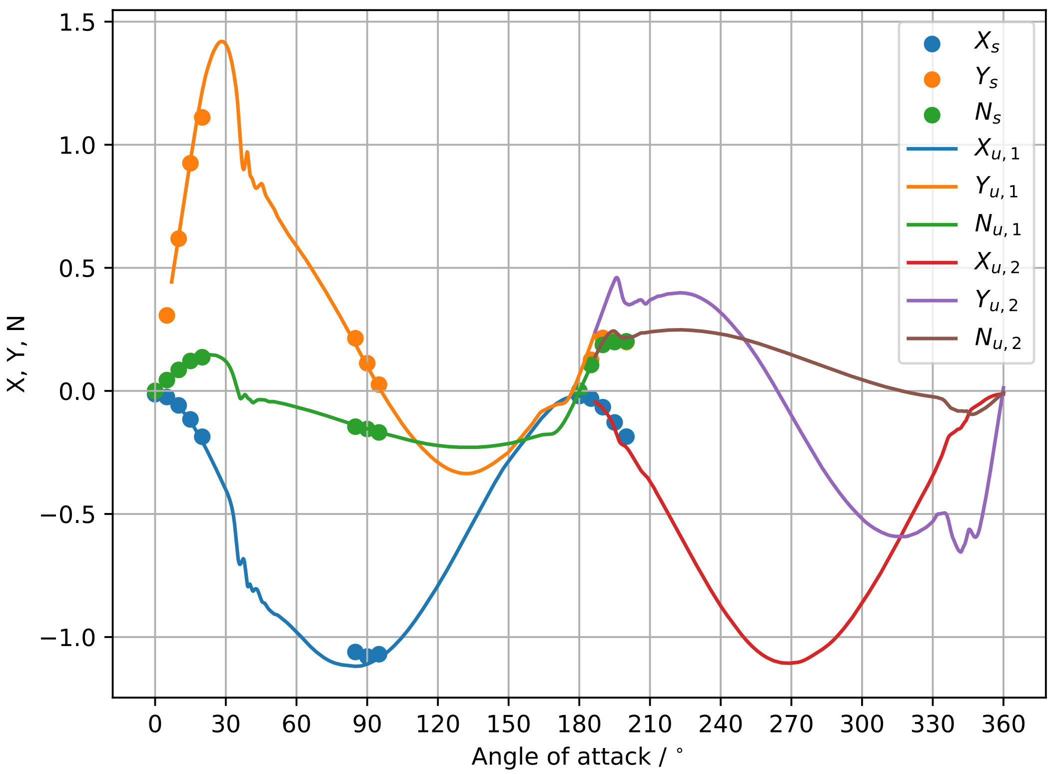

Figure 9 – Comparison of the steady ($_s$) and unsteady ($_{u,}$) longitudinal force (X), lateral force (Y) and yawing moment (N).

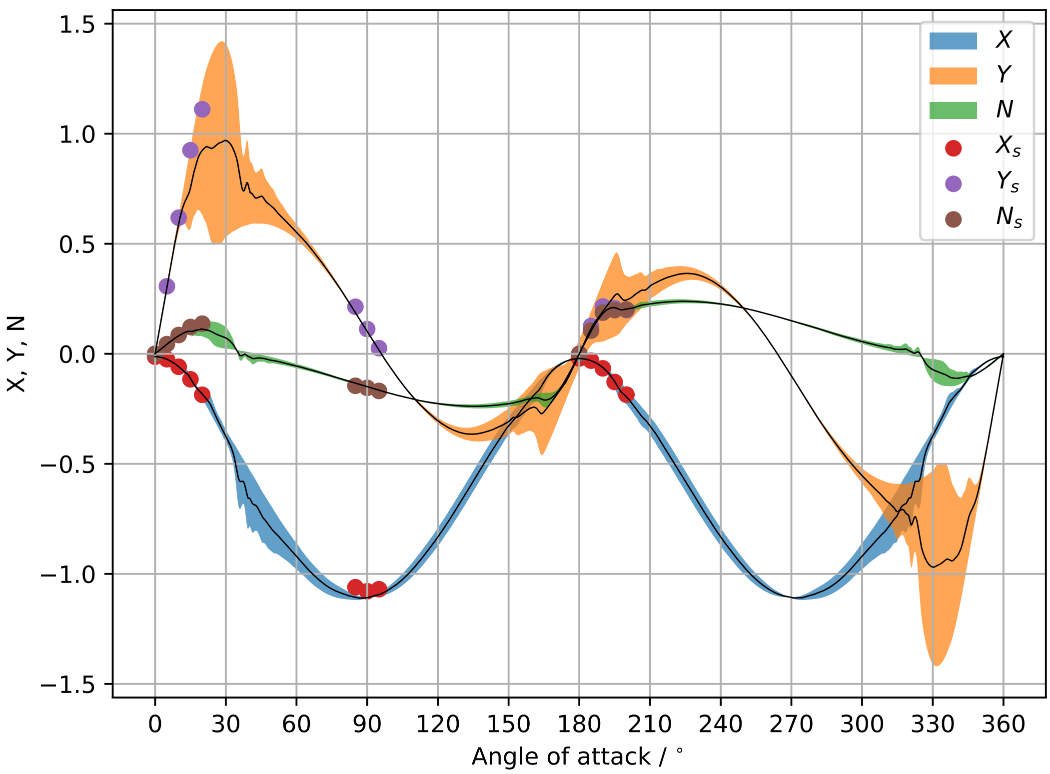

Figure 10 – Comparison of the steady ($_s$) and unsteady ($_{u,}$) longitudinal force (X), lateral force (Y) and yawing moment (N).

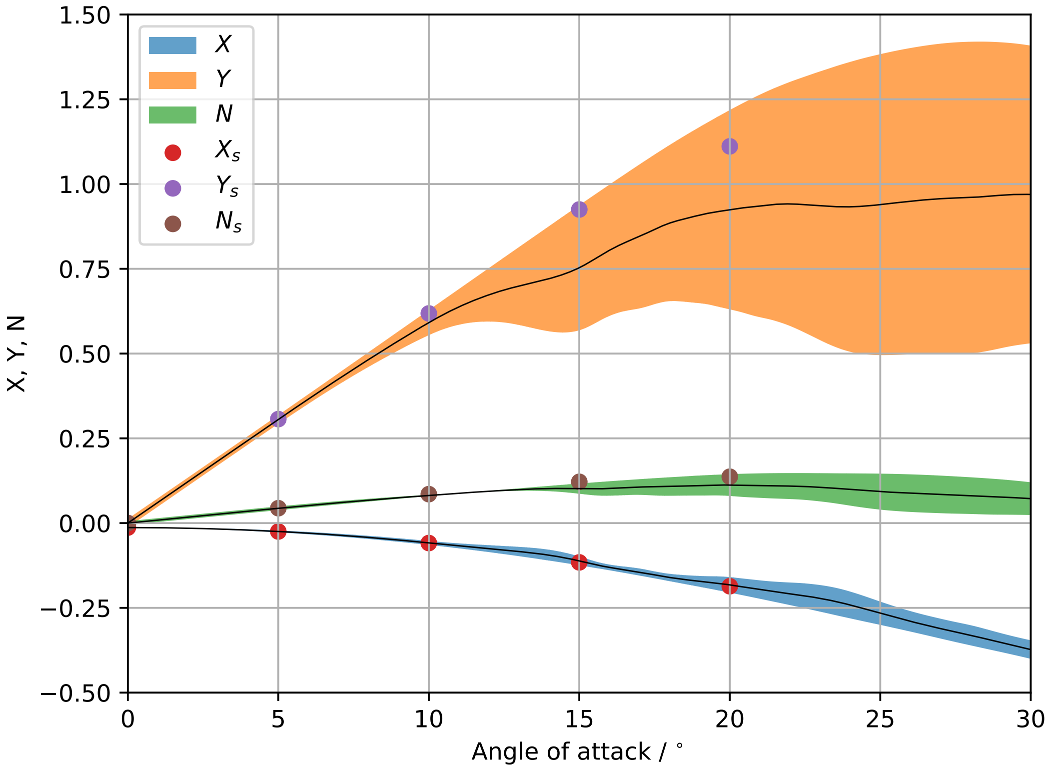

Figure 11 – Comparison of the steady and unsteady longitudinal force (X), lateral force (Y) and yawing moment (N) from $\alpha = 0°$ to $30°$.

The final results for the three coefficients are interpolated to a $1°$ and a $5°$ interval. Both coefficient sets are shown in Fig. 12 and the latter set is listed in Appendix A1.

The maximum lift coefficient $C_{L,max}$ in normal flow condition is approximately $C_{L,max} = 0.97$ (attained at α = $30°$), while for reverse flow conditions, $C_{L,max} = 0.27$, at α = $196°$. The lift curve slope C_{L_α} in normal flow conditions is found to be $C_{L_\alpha}|_{0°} = 3.51\,\text{rad}^{-1} = 0.0612\,1/°$. For the reverse flow condition, it is significantly smaller at $CLa|_{180°} = 1.33\,\text{rad}^{-1} = 0.0232\,1/°$. A comparison of the minimum drag coefficient $C_{D,min}$ (both at $\alpha = 0°$ and $180°$), shows that the expected behaviour is found: for normal flow conditions it equals $C_{D,min}|_{0°} = -0.013$, while in reverse flow condition it is higher at $C_{D,min}|_{180°} = -0.021$. In section 1.3.2, a theoretical estimate (3.55) was computed for the lift curve slope near $\alpha = 0°$ using planform data and the two-dimensional lift curve slope obtained with XFOIL. The above CFD result (3.51) is very close to the theoretical value. This shows qualitatively correct values in normal flow conditions and quantitatively correct behaviour over the full range of angles of attack. Obviously, switching to a more sophisticated turbulence modelling approach such as Detached Eddy Simulation (DES) or Large Eddy Simulation (LES) may improve results in deep stall conditions, but this would also have a price as those computations require significantly finer grids and thus more computational resources.

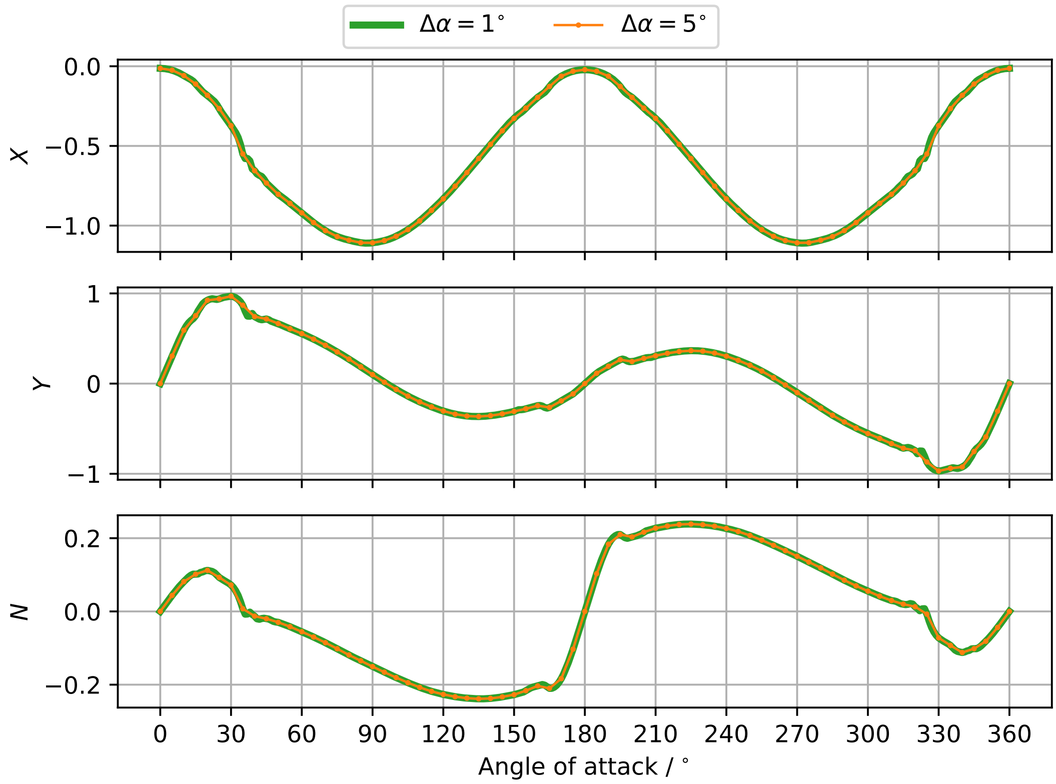

Figure 12 – Longitudinal force (X), lateral force (Y) and yaw moment (N) coefficients interpolated with $1°$ and $5°$ increments.

3 Conclusions

This report documents recent research to compute the open-water rudder characteristics for the rudder of a suction hopper dredger (H40) for which FH is developing a manoeuvring model. The numerical setup uses FINE/Marine to compute the lift, drag and yawing moment on an isolated rudder with a symmetry plane at its top side. Unsteady computations were used to obtain coefficient values for the full range of angles of attack, by slowly rotating the rudder around its stock. To account for hysteresis near stall, the results of two data sets (one with increasing angle of attack and the second one with decreasing angle of attack) are averaged to obtain the final results. Due to the lateral symmetry of the rudder, a single computation is sufficient that covers the complete range of angles of attack (from $\alpha = 0°$ to $360°$).

Due to an unexpected crash of the first unsteady computation shortly after $\alpha = 180°$ was reached, a second computation was configured to generate the remainder of the rudder forces. For these two computations, approximately 4.2 days of computing time were required using approximately 100 cores (112 for the first computation and 96 for the second computation).

The results are shown to be qualitatively correct over the full range of angles of attack and for the attached flow condition, the agreement between the numerically obtained lift curve slope and a theoretical estimate is very good.

References

Leishman, **J. G.** (2023). Introduction to Aerospace Flight Vehicles. Embry-Riddle Aeronautical University. ISBN: 9798985261400

Van Hoydonck, **W.; Delefortrie**, **G.; De Maerschalck**, **B.; Vantorre**, **M.** (2018). Open-Water Rudder Tests using CFD. ***in**: proceedings of the 32nd Symposium on Naval Hydrodynamics, Hamburg, Germany, 5–10 August 2018*

Van Kerkhove, **G.; Vantorre**, **M.; Delefortrie**, **G.** (2009). Advanced Model Testing Techniques for Ship Behaviour in Shallow and Confined Water. *Proceedings of The First International Conference on Advanced Model Measurement Technology for the EU Maritime Industry*: 29 pp.

Vantorre, **M.** (2001). Stationary and non-stationary open water rudder tests. ***in**:* Kijima, K. (Ed.). *Mini Symposium on Prediction of Ship Manoeuvring Performance, 18 October 2001, Tokyo, Japan.* Japan Marine Dynamics Research Sub-Committee. 103–111 pp.

A1 Coefficient values

The numerical values of the longitudinal force (X), lateral force (Y) and yawing moment (N) coefficients interpolated to a five degree increment are shown in the listing below.

Listing A1.1 – Coefficient values interpolated to five degree increment.

```
# density: 999.1026 kg/m^3
# Lref: 3.9 m
# draft: 5.4 m
# Vref: 5 m/s
# Fndim: 0.5 * density * Vref^2 * Lref * draft
# Mndim: 0.5 * density * Vref^2 * Lref^2 * draft
AoA,X,Y,N
0.0,-0.01313382259967305,2.2802025962326968e-06,3.3417728157437085e-07
5.0,-0.02467623530222579,0.3056753257522331,0.04367625465145055
10.0,-0.05842605693430174 4,0.5912699354989952,0.08146488137385481
15.0,-0.1114552852082782 7,0.7531592900755393,0.1016624404175656 8
20.0,-0.18215896372437665,0.9242609436418443,0.1122111161677581 4
25.0,-0.2658303125531985,0.9392299901868933,0.09279375426700445
30.0,-0.37299292468790174,0.9692652131174095,0.07214786355978547
35.0,-0.5503244272969948,0.8690611792055035,0.007311957042872295
40.0,-0.6553496419489059,0.742528996060340 6,-0.01278013763464198 2
45.0,-0.7330997031520672,0.716593746987333,-0.01999499436294343 4
50.0,-0.8037506753574594,0.6654416046124252,-0.02970393180168619
55.0,-0.8604073260066737,0.6083025160669856,-0.04161620544404394
60.0,-0.9199533680932918,0.5541911690731283,-0.05542544995052873
65.0,-0.980812384117756,0.49343824265310693,-0.06981861732754174
70.0,-1.031714719683209,0.42535759004348306,-0.0852877414875818
75.0,-1.0689311281078158,0.35107408090262254,-0.10189965333307863
80.0,-1.09157358662285,0.2716036178413917,-0.11897294017843131
85.0,-1.1075271348585318,0.18594305786223903,-0.13476110835420216
90.0,-1.1081528270169552,0.0998657041251393,-0.15060254404542794
95.0,-1.094354955357648,0.015377794270728343,-0.1659441276514971
100.0,-1.0670666953773595,-0.06509856862682849,-0.18062757140006167
105.0,-1.025526186443652,-0.1388800527215613,-0.194606046229679 4
110.0,-0.9704622214200593,-0.20333201177614643,-0.20738919402888426
115.0,-0.9044358182127749,-0.2579119509565761,-0.2182558788035457
120.0,-0.8323132085475554,-0.30451538872489753,-0.22659617677706395
125.0,-0.7524671282648837,-0.3387647140320197,-0.23283181324223348
130.0,-0.6671958651277979,-0.35954043373031164,-0.23679194130176395
135.0,-0.5788407021253706,-0.3651570596050987,-0.2386120695089387
140.0,-0.49019322294026796,-0.35576120574876774,-0.23747017493813746
145.0,-0.405010605414675,-0.3359250115716283,-0.2333366501109080 7
150.0,-0.32722989349650905,-0.3088062890907075,-0.22724195646778772
155.0,-0.2628734253349275,-0.27914756248650824,-0.2163592708618711
160.0,-0.19519752510884944,-0.24432790368746876,-0.2033460231940797
165.0,-0.12678136507032728,-0.2645898785982615,-0.21004158740177442
170.0,-0.0624424037338479 7,-0.1921571358760927,-0.1835436784926893
```

```
175.0,-0.03144078651363579,-0.1146910733286913,-0.10294043683077302
180.0,-0.02149586192148082,9.198058455946352e-07,7.9201847170707e-07
185.0,-0.031440857144146246,0.11469142869014422,0.10294078017200936
190.0,-0.06244299103788847,0.192158202990846 8,0.1835444377360677
195.0,-0.1267820748584913,0.26459034684275445,0.21004151452350744
200.0,-0.1951982354403903,0.2443279121940852 8,0.20334622638343458
205.0,-0.2628741093819227,0.2791479638146832 6,0.2163594517183339
210.0,-0.32723098153813596,0.3088069206203474,0.22724207834651 7
215.0,-0.4050114157033027,0.3359252491867752 4,0.2333367039303229
220.0,-0.49019357785259815,0.3557612683304859,0.23747018610356338
225.0,-0.578841668708788,0.3651570839080579,0.23861206140945349
230.0,-0.6671963163059197,0.3595403598847153,0.2367919282982661
235.0,-0.7524680363012368,0.338764416510275,0.2328317551025582 4
240.0,-0.8323137805338421,0.3045150884651532,0.2265961240578166
245.0,-0.904436343586557,0.2579115747467325,0.2182558120950633 7
250.0,-0.9704626765917429,0.2033315655878204,0.20738910364031263
255.0,-1.0255265421539792,0.13887953186508245,0.1946059440988162 6
260.0,-1.0670669466997669,0.0650979844146926 5,0.1806274589141704
265.0,-1.0943553064869442,-0.015379382748548309,0.16594384198718767
270.0,-1.1081528841434445,-0.0998663360155186,0.15060242439106664
275.0,-1.1075268915267946,-0.18594471463225284,0.13476080080842587
280.0,-1.0915734476007721,-0.27160424349856 37,0.11897281630956193
285.0,-1.0689309080076135,-0.3510746456371413,0.10189952327552326
290.0,-1.0317143731729697,-0.4253581191702847,0.08528761878563186
295.0,-0.9808119382887669,-0.49343873264313554,0.06981850784131435
300.0,-0.9199529454468649,-0.5541916075379527,0.05542534231897456 4
305.0,-0.8604067063700008,-0.6083031436418681,0.04161605921702879
310.0,-0.8037503233821448,-0.6654418141506772,0.029703903998315673
315.0,-0.7330984613026411,-0.7165936250924163,0.019994902129149287
320.0,-0.655349564492469,-0.7425298592564538,0.012780057207016037
325.0,-0.5503218525556327,-0.8690637754029403,-0.007312947511993839
330.0,-0.37299136976876035,-0.9692654004442153,-0.07214831884003903
335.0,-0.26582923744415976,-0.9392295703391683,-0.09279398266927853
340.0,-0.18215804353031273,-0.9242599348826183,-0.1122112143102103 2
345.0,-0.1114545241883643,-0.7531576524604996,-0.10166249732640355
350.0,-0.05842547272154835,-0.5912665490046985,-0.08146446067798484
355.0,-0.024676155826397376,-0.30567425335354537,-0.043676104949277844
360.0,-0.013133822379572849,0.0,0.0
```

DEPARTMENT **MOBILITY & PUBLIC WORKS**
Flanders Hydraulics

Berchemlei 115, 2140 Antwerp
T +32 (0)3 224 60 35
F +32 (0)3 224 60 36
waterbouwkundiglabo@vlaanderen.be
www.flandershydraulics.be